Molecular dynamics simulations of binary structure H hydrogen and methyl-tert-butylether clathrate hydrates

Saman Alavi, J. A. Ripmeester, and D. D. Klug

Citation: The Journal of Chemical Physics **124**, 204707 (2006); doi: 10.1063/1.2199850
View online: http://dx.doi.org/10.1063/1.2199850
View Table of Contents: http://scitation.aip.org/content/aip/journal/jcp/124/20?ver=pdfcov
Published by the AIP Publishing

Molecular dynamics simulations of binary structure H hydrogen and methyl-*tert*-butylether clathrate hydrates

Saman Alavi,[a] J. A. Ripmeester, and D. D. Klug
Steacie Institute for Molecular Sciences, National Research Council of Canada, 100 Sussex Drive, Ottawa, Ontario K1A 0R6, Canada

(Received 23 February 2006; accepted 30 March 2006; published online 25 May 2006)

Binary structure H (sH) hydrogen and methyl-*tert*-butylether (MTBE) clathrate hydrates are studied with molecular dynamics simulations. Simulations on a $3\times3\times3$ sH unit cell with up to 4.7 mass % hydrogen gas are run at pressures of 100 bars and 2 kbars at 100 and 273 K. For the small and medium cages of the sH unit cell, H_2 guest molecule occupancies of 0, 1 (single occupancy), and 2 (double occupancy) are considered with the MTBE molecule occupying all of the large cages. An increase of the small and medium cage occupancies from 1 to 2 leads to a jump in the unit cell volume and configurational energy. Calculations are also set up with 1/3, 2/3, and 8/9 of the MTBE molecules in the large cages replaced by sets of three to six H_2 molecules, and the effects on the configurational energy and volume of the simulation cell are determined. As MTBE molecules are replaced with sets of H_2 guests in the large cages, the configurational energy of the unit cell increases. At the lower temperature, the energy and volume of the clathrate are not sensitive to the number of hydrogen guests in the large cages; however, at higher temperatures the repulsions among the H_2 guest molecules in the large cages cause an increase in the system energy and volume.
 [DOI: 10.1063/1.2199850]

I. INTRODUCTION

Structure H (sH) clathrate hydrates crystallize in a hexagonal $P6/mmm$ space group with a unit cell containing 34 water molecules.[1–3] The water framework of the unit cell consists of three 12-sided $[5^{12}]$ "small" (s) polyhedral cages, two 12-sided $[4^3 5^6 6^3]$ "medium" (m) polyhedral cages, and one 18-sided $[5^{12}6^8]$ "large" (ℓ) polyhedron cage. The polyhedra of the structure H clathrate are shown in Fig. 1. The structure H clathrate forms to accommodate large guest molecules such as 2,2-dimethylpentane, cycloheptane, or methyl-*tert*-butylether (MTBE).

The structure II (sII) pure hydrogen and binary hydrogen+tetrahydrofurane (THF) clathrates have been recently synthesized and studied experimentally with Raman and NMR techniques and theoretically with molecular dynamics simulations. The hydrogen clathrates[4,5] have been proposed as candidates for hydrogen storage.[6] The synthesis of the sII hydrogen clathrates requires high pressures in the range of 180–600 MPa. At these high pressures, the hydrogen clathrates are stable up to room temperature.[4] At ambient pressure (0.1 MPa), the pure hydrogen clathrate is stable for temperatures lower than 140 K.[6] The hydrogen-to-water weight percentages for the pure hydrogen clathrate have been estimated to be between 3.9 and 5.2 wt %,[4] depending on whether the small cages in the sII clathrate are singly or doubly occupied by hydrogen guests.[7] The binary H_2/THF clathrate can be synthesized at lower pressures of ~15 MPa.[8,9] The hydrogen carrying capacity for this clathrate was measured to be 2.1–4.0 wt % which corresponds to some hydrogen guest molecules occupying large cages in the sII clathrate structure.

There is recent experimental evidence for formation of mixed structure H clathrates of large water insoluble solutes with hydrogen.[10] At high pressures, the Raman adsorption of the hydrogen guests is split into two peaks with a separation of $\approx$10 cm^{-1} and both peaks are redshifted with respect to the free hydrogen gas Raman vibron peak of 4155 cm^{-1}. This provides some evidence that the hydrogen guest molecules occupy the small, medium, and large cages. Quantitative aspects of the adsorption are subject to some experimental uncertainty. Most importantly from a practical point of view, the total hydrogen content and the distribution of the hydrogen guests among the cages are not known. Theoretically exploring structural and energetic aspects of the structure H clathrate with different hydrogen contents and distributions can be valuable as a guide for future experimental work on this clathrate. In particular, the radial distribution functions determined from the simulations may be of use in interpreting crystallographic information on this system.

In this work, we use molecular dynamics (MD) simulations to study binary hydrogen+MTBE sH clathrates. In particular, we are interested in comparing binary clathrates with different H_2:MTBE ratios. This work is a continuation of our previous molecular dynamics study of hydrogen storage in pure hydrogen clathrate and binary hydrogen/THF compounds.[11]

II. COMPUTATIONAL METHODS

In the molecular dynamics simulations, the extended simple point charge (SPC/E) model[12] is used for water, and

[a]Electronic mail: saman.alavi@nrc.ca

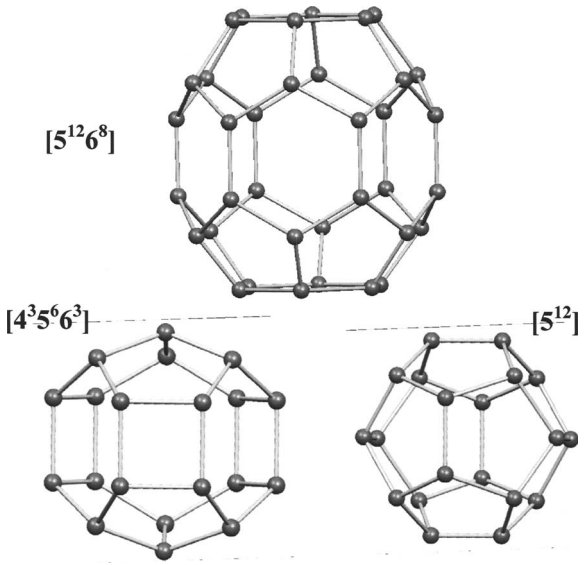

FIG. 1. The $[5^{12}6^8]$, $[4^35^66^3]$, and $[5^{12}]$ cages of the structure H unit cell.

the H_2 guest molecules are considered rigid with a bond length of 0.7414 Å which corresponds to the experimental gas-phase value.[13] The details of the H_2O and H_2 force fields are identical to those of our previous work on pure sII hydrogen clathrates.[11,14] The MTBE guest molecules are considered to be flexible in the MD simulations. The initial structure of the MTBE molecule was determined by energy optimization using density functional theory at the B3LYP/6-311++G(d,p) level[15] with the GAUSSIAN 98 suite of programs.[16]

The intermolecular potentials between atoms on molecules i and j used in the simulations have the form

$$V(\text{inter}) = \sum_{i=1}^{N-1} \sum_{j>i}^{N} \left\{ 4\varepsilon_{ij}^0 \left[\left(\frac{\sigma_{ij}^0}{r_{ij}} \right)^{12} - \left(\frac{\sigma_{ij}^0}{r_{ij}} \right)^{6} \right] + \frac{q_i q_j}{4\pi\varepsilon_0 r_{ij}} \right\}, \quad (1)$$

where the first term is the Lennard-Jones potential which models the van der Waals interactions in the system and the second term represents the electrostatic intermolecular interactions of atoms i and j which carry electrostatic charges q_i and q_j. Electrostatic charges on the atoms of the MTBE molecule are estimated by using the charges from an electrostatic potential grid (CHELPG) method[17] as implemented in the GAUSSIAN 98 program. The van der Waals interaction parameters for the atoms in MTBE molecule were assigned according to the classification of the general AMBER force field (GAFF).[18] The Lennard-Jones potential was chosen to represent van der Waals interactions between the MTBE atoms and the cage water and hydrogen guest molecules. The standard combination rules, $\varepsilon_{ij}^0=(\varepsilon_{ii}^0\varepsilon_{jj}^0)^{1/2}$ and $\sigma_{ij}=(\sigma_{ii}+\sigma_{jj})/2$, were used for the Lennard-Jones potential parameters between unlike atom-type force centers i and j. The values of the intermolecular potential parameters used in the simulations are given in Table I. The numbering of the atoms of the MTBE molecule is shown in Fig. 2.

The intramolecular potential used for MTBE has the form

TABLE I. Atomic charges and Lennard-Jones interaction parameters for SPC/E water, rigid H_2, and MTBE used in the MD simulations.

Atom (assignment)	q (e)	σ_{ii}^0 (Å)[a]	ε_{ii}^0 (kJ/mol)[a]
O (water)	−0.847 6	3.166	0.650 2
H (water)	+0.423 8	0.000	0.000 0
H (guest)	+0.493 2	0.000	0.000 0
HCM (guest)[b]	−0.986 4	3.038	0.285 2
C1 (C3)	+0.102 732	3.3996	0.457 73
H1–H3 (H1)	+0.025 647	2.4714	0.065 69
O (OS)	−0.540 494	3.0000	0.711 28
C2 (C3)	+0.772 121	3.3996	0.457 73
C3–C5 (C3)	−0.347 427	3.3996	0.457 73
H4–H12 (HC)	+0.070 109	2.6496	0.065 69

[a]The intermolecular potential parameters between unlike atoms are determined from combination rules.
[b]Corresponds to the center of mass of the H_2 molecule.

$$V(\text{intra}) = \sum_{\text{bonds}} \frac{k_r}{2}(r-r_{\text{eq}})^2 + \sum_{\text{angles}} \frac{k_\theta}{2}(\theta-\theta_{\text{eq}})^2 + \sum_{\text{dihedrals}} \sum_{i=1}^{3} \frac{V_i}{2}[1+(-1)^{i-1}\cos(i\phi-\Phi)], \quad (2)$$

where k_r, k_θ, and V_i are the bond stretch, angle bending, and torsional angle force constants, respectively, and r_{eq} and θ_{eq} are the equilibrium bond lengths and bond angles, respectively. The values of the intramolecular potential parameters of Eq. (2) for MTBE were assigned according to the classification of the GAFF (Ref. 18) and are given in Table II.

Isotropic constant-pressure–constant-temperature molecular dynamics simulations with the Nosé-Hoover barostat algorithm[19,20] and the modification of Melchionna *et al.*[21] on a $3\times3\times3$ ($36.99\times36.99\times29.76$ Å^3 initial dimensions) sH clathrate hydrate supercell with periodic boundary conditions were performed with the DLPOLY program version 2.14.[22] The relaxation times for the thermostat and barostat were chosen as 0.5 and 2.0 ps, respectively. The equations of motion were integrated with a time step of 1 fs using the Verlet leapfrog scheme.[23–25] Coulombic long-range interactions were calculated using the Ewald summation method[23–25] with a precision of 1×10^{-6}, and all intermolecular interactions in the simulation box were calculated within a cutoff distance of $R_{\text{cutoff}}=13.0$ Å. The simulations were carried out for a total time of 80 ps, with the first 30 ps used for tem-

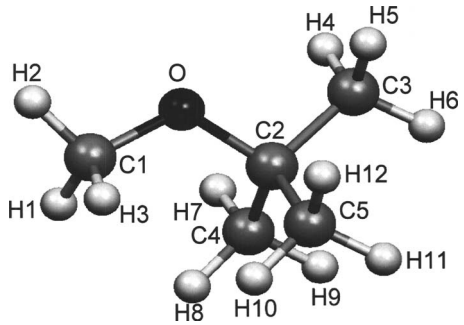

FIG. 2. Numbering scheme used for MTBE. The atomic labels for each atom according to the convention of the general AMBER force field are given in Table I.

TABLE II. GAFF intramolecular potential parameters for MTBE. The numbers of bond, angle, and dihedral interactions are given in parentheses after the description of the interaction type.

Bonds	k_r (kJ/mol Å^2)	r_{eq} (Å)	
C3–H1 (3)	2810.8	1.093	
C3–H3 (9)	2822.5	1.092	
C3–OS (2)	2523.0	1.439	
C3–C3 (3)	2536.3	1.535	
Harmonic angles	k_θ (kJ/mol rad^2)	θ_{eq} (deg)	
H1–C3–H1 (3)	328.0	109.55	
H1–C3–OS (3)	425.1	108.82	
HC–C3–HC (9)	388.3	110.5	
HC–C3–C3 (9)	329.7	108.35	
C3–OS–C3 (1)	519.6	113.41	
OS–C3–C3 (3)	567.4	108.42	
C3–C3–C3 (3)	528.9	110.63	
Dihedral angles	V_i	Φ	i
H1–C3–OS–C3 (3)	0.80	0.00	3
OS–C3–C3–HC (9)	0.52	0.00	1
C3–C3–C3–HC (18)	0.33	0.00	3
C3–OS–C3–C3 (3)	0.80	0.00	3

perature scaled equilibration. For dynamic calculations of the guests in the cages, including mean-square displacements and velocity-autocorrelation functions, *NVE* simulations where performed on systems previously equilibrated with the *NPT* simulations described above. The simulations where run for a further 30 ps and dynamical averages were calculated with data from the final 20 ps of the simulations.

The initial structures for clathrate cages were chosen as described in Refs. 11 and 14 based on the experimental x-ray crystallography of the sH clathrate.[1–3] The hydrogen atoms of the water molecules are disordered in the sH clathrate and

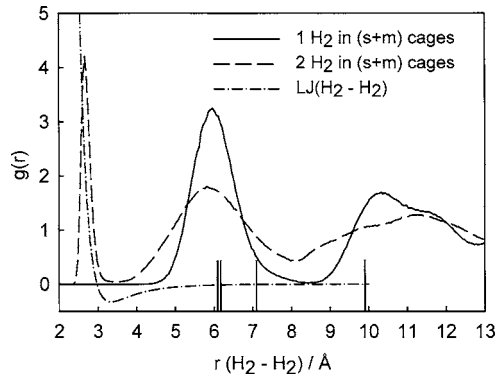

FIG. 3. The H_2-H_2 center-of-mass RDF for hydrogen guest molecules for singly and doubly occupied small ($[5^{12}]$ or *s*) and medium ($[4^35^66^3]$ or *m*) cages at 150 K and 2 kbar pressure. In the doubly occupied (*s*+*m*) case, 1/3 of the large cages were occupied by four H_2 molecules. The separations 6.106, 6.165, 7.119, and 9.921 Å which correspond to the separations of the centers of the *s*-*s*, *s*-*m*, *m*-*m*, and second nearest neighbor *s*-*s* cages are indicated by vertical lines on the *x* axis. The H_2-H_2 center-of-mass Lennard-Jones potential (with arbitrary vertical scale) is shown for reference. In doubly occupied cages the two guest hydrogen molecules are confined into the repulsive region of the Lennard-Jones potential.

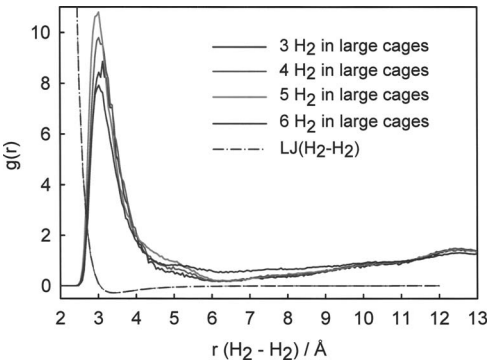

FIG. 4. The H_2-H_2 center-of-mass RDF for three to six hydrogen guest molecules in 2/3 of the large ($[5^{12}6^8]$ or *l*) cages at 150 K and 2 kbar pressure. The H_2-H_2 center-of-mass Lennard-Jones potential (with arbitrary vertical scale) is shown for reference. The distributions of the hydrogen molecules in the large cages fall in both the attractive and repulsive regions of the Lennard-Jones potential.

a Monte Carlo calculation was used to distribute the hydrogen atoms among the oxygen sites of the clathrate lattice subject to the constraints of the Bernal and Fowler ice rules.[26] The distribution of the hydrogen atoms that gave the minimum total dipole moment of the unit cell of the sH lattice was chosen as the initial state for the molecular dynamics simulations.

In the first set of calculations, all 27 large cages of the simulation cell were occupied by MTBE molecules and zero, one, or two hydrogen guest molecules were placed in each small and medium cages. A second series of calculations was performed where 1/3, 2/3, or 8/9 of the 27 large cages were occupied by sets of three to six H_2 guest molecules and the remaining large cages retained the MTBE molecules. Given the distances of adjacent large cages and the 13.0 Å cutoff for the intermolecular potentials, interactions between guests in neighboring large cages are small and the random placement of the MTBE guest molecules among large cages should be sufficient to give representative values of thermodynamic quantities. The oxygen atoms of the MTBE molecule were originally placed in the center of the large cages and their positions and orientations were equilibrated during the simulation.

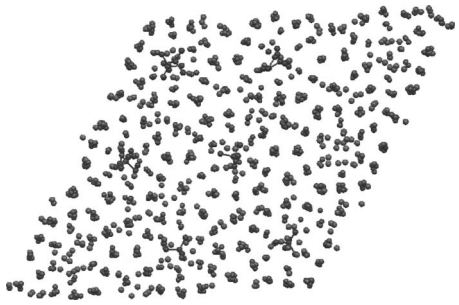

FIG. 5. A snapshot of the MTBE+H_2 structure H clathrate with the hydrogen atoms removed for clarity. The oxygen atoms are shown by red spheres, the carbon atoms by green spheres, and the center or mass of the H_2 guest molecules by the blue spheres. In this configuration, 2/3 of the MTBE molecules in the large cages have been substituted with sets of five H_2 molecules.

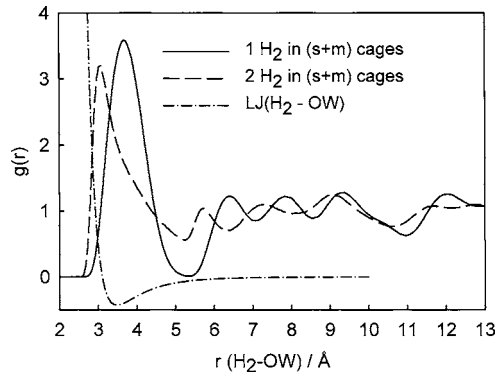

FIG. 6. The H_2–OW RDF for hydrogen guest molecules for singly and doubly occupied small (s) and medium (m) cages at 150 K and 2 kbar pressure. The distance of the center of the small cages to the oxygen atoms ranges between 3.86 and 4.02 Å and the distance of the center of the medium cages to the oxygen atoms ranges between 3.78 and 4.10 Å. These spreads correspond to the position of the first band in the singly occupied RDF. The H_2–OW Lennard-Jones potential (with arbitrary vertical scale) is shown for reference. In the singly occupied cages, the interactions of the guest hydrogen molecules with the cage oxygens are predominantly attractive, but in the doubly occupied cages, the broad first peaks show that the guests have attractive and repulsive interactions with the oxygen atoms of the cage water molecules.

III. RESULTS

The radial distribution functions for the singly and doubly occupied hydrogen guest molecules in the small and medium cages (and large cages occupied by MTBE) are shown in Fig. 3. The H_2–H_2 center-of-mass Lennard-Jones intermolecular potential is shown in this figure for reference. For the singly occupied case, the locations of the peaks in the radial distribution function (RDF) plots correspond to the distances expected from placing the guest molecules near the center of the s and m cages. The distances between the centers of the small and medium cages are shown by small vertical lines in Fig. 3. In the singly occupied ($s+m$) case, the H_2 guests in adjacent cages have weak attractive interactions. For doubly occupied s and m cages, the peak in the H_2–H_2 RDF at 2.67 Å is related to the two H_2 guest molecules in the same cage. In this case, the separation between these two hydrogen molecules is such that they are mostly confined to the repulsive segment of the Lennard-Jones potential.

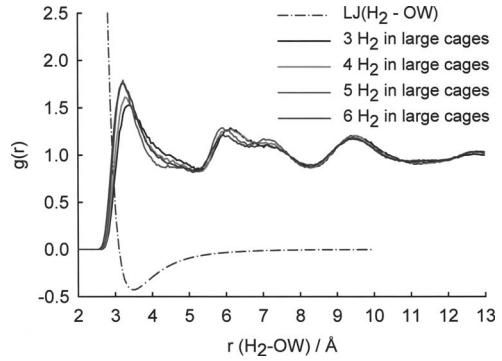

FIG. 7. The H_2–OW RDF for three to six hydrogen guest molecules in 2/3 of the large (ℓ) cages at 150 K and 2 kbar pressure. The H_2–OW Lennard-Jones potential (with arbitrary vertical scale) is shown for reference. The broad first peaks show that the guests have attractive and repulsive interactions with the oxygen atoms of the cage water molecules.

TABLE III. The configurational energy (kJ/mol) of binary structure H clathrates with different hydrogen contents along with the corresponding error bars of the calculations in parentheses for three temperature/pressure conditions. The weight percent of H_2 guest for each configuration is also given.

Temperature/pressure		150 K/2 kbars	150 K/100 bars	273 K/100 bars
H_2 content	wt % H_2	E_{config}	E_{config}	E_{config}
$0(s+m)+0\ell$[a]	0	−2013(2)	−2011(2)	−1839(5)
$1(s+m)+0\ell$[a]	1.410	−2051(3)	−2047(3)	−1879(6)
$1(s+m)+3\ell$[b]	1.759	⋯	−2015(2)	−1852(4)
$1(s+m)+4\ell$[b]	1.855	⋯	−2018(2)	−1853(4)
$1(s+m)+5\ell$[b]	1.951	⋯	−2017(3)	−1848(5)
$1(s+m)+6\ell$[b]	2.047	⋯	−2015(3)	−1850(5)
$1(s+m)+3\ell$[c]	2.138	⋯	−1986(3)	−1832(6)
$1(s+m)+4\ell$[c]	2.337	⋯	−1989(3)	−1822(5)
$1(s+m)+5\ell$[c]	2.535	⋯	−1990(3)	−1830(5)
$1(s+m)+6\ell$[c]	2.733	⋯	−1983(3)	−1826(5)
$1(s+m)+3\ell$[d]	2.409	⋯	−1966(3)	−1818(5)
$1(s+m)+4\ell$[d]	2.681	⋯	−1964(2)	−1817(4)
$1(s+m)+5\ell$[d]	2.951	⋯	−1972(3)	−1819(5)
$1(s+m)+6\ell$[d]	3.220	⋯	−1965(3)	−1810(5)
$2(s+m)+0\ell$[a]	2.819	−2011(3)	−2004(3)	−1979(8)
$2(s+m)+3\ell$[b]	3.179	−1982(2)	−1976(3)	−1792(7)
$2(s+m)+4\ell$[b]	3.272	−1981(3)	−1975(5)	−1784(8)
$2(s+m)+5\ell$[b]	3.365	−1982(3)	−1975(3)	−1774(8)
$2(s+m)+6\ell$[b]	3.458	−1977(3)	−1970(3)	−1748(13)
$2(s+m)+3\ell$[c]	3.611	−1954(3)	−1948(3)	−1777(6)
$2(s+m)+4\ell$[c]	3.804	−1955(3)	−1948(3)	−1777(7)
$2(s+m)+5\ell$[c]	3.996	−1955(3)	−1948(3)	−1764(6)
$2(s+m)+6\ell$[c]	4.187	−1940(3)	−1938(4)	−1741(11)
$2(s+m)+3\ell$[d]	3.919	−1935(3)	−1930(4)	−1766(6)
$2(s+m)+4\ell$[d]	4.182	−1937(3)	−1928(3)	−1767(7)
$2(s+m)+5\ell$[d]	4.444	−1938(3)	−1931(3)	−1748(6)
$2(s+m)+6\ell$[d]	4.705	−1920(3)	−1916(3)	−1720(13)

[a]Large cages all occupied by MTBE.
[b]1/3 of large cages occupied by H_2 guests, 2/3 by MTBE.
[c]2/3 of large cages occupied by H_2 guests, 1/3 by MTBE.
[d]8/9 of large cages occupied by H_2 guests, 1/9 by MTBE.

Calculations are performed in which 1/3, 2/3, and 8/9 of the MTBE molecules in the large cages are replaced with sets of H_2 guest molecules, with either one or two hydrogen guests in the small and medium cages. This obviously increases the hydrogen storage of the clathrate above the case where MTBE occupies all the large cages. The RDFs for hydrogen guest molecules in the large cages for the particular case where 2/3 of the large cages are occupied by sets of three to six H_2 guest molecules rather than MTBE molecules are shown in Fig. 4. In this case, the ($s+m$) cages each have two H_2 guests. The H_2–H_2 Lennard-Jones potential is also shown for reference. The average cavity radius of the large cages is 5.7 Å,[3] and within this cavity up to six H_2 guest molecules can be accommodated such that their most probable separation is ≈3 Å. The distributions of the hydrogen guest centers in the large cages are broad which reflects the size of the cages. A considerable component of the distribution falls on the attractive region of the Lennard-Jones potential. A snapshot of the final configuration for the simulation with five H_2 guests in 2/3 of the large cages is shown in Fig. 5.

The H_2 center-of-mass–water-oxygen (H_2–OW) RDF

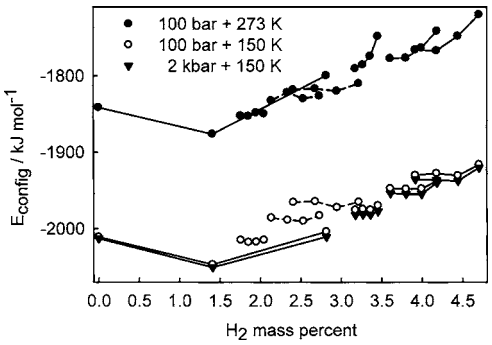

FIG. 8. The total unit cell configurational energy (kJ/mol) for various MTBE+H_2 binary clathrates at 150 and 273 K temperatures and 100 bar and 2 kbar pressures for different occupancies of the cages with H_2 guests. The distribution of hydrogen guest molecules among the cages that corresponds to each hydrogen mass percent is given in Table III. Points with single occupancy of the $(s+m)$ cages are connected with dashed lines and points with double occupancy of the $(s+m)$ cages of the large cages are connected with solid lines.

for single and double occupancies in the *s* and *m* cages is shown in Fig. 6, with the H_2–OW Lennard-Jones potential given for reference. The average cavity radii for the *s* and *m* cages are 3.9 and 4.1 Å, respectively,[3] and these distances correspond with the first broad maximum in the RDF for the singly occupied case. The H_2–OW separations mostly fall in the attractive region of the Lennard-Jones potential. In the doubly occupied case, the repulsions among the H_2 guests push the maximum in the H_2–OW RDF to a distance of about 3 Å which falls in the repulsive region of the H_2–OW Lennard-Jones potential.

The H_2–OW RDF for three to six hydrogen guests in the large cages are shown in Fig. 7 (with 2/3 substitution of the MTBE in the large cages). The RDF curves for these four large cage occupancies are similar and the first peak lies at a separation of ≈3.2 Å. This figure and Fig. 4 suggest that the three to six H_2 guest molecules cluster in the center of the large cages and have similar interactions with the cage oxygen atoms.

The configurational energies (sum of intermolecular and intramolecular potentials) of the unit cell for various MTBE and H_2 occupancies are given in Table III and plotted in Fig. 8. Calculations were preformed for single and double occupancies of the $(s+m)$ cages with all the large cages occupied by MTBE and for cases where 1/3, 2/3, and 8/9 of the large cages are occupied by sets of three to six H_2 guests. There is

TABLE IV. Unit cell volume (Å^3) and density (g/cm^3) of binary sH clathrates with different H_2 guest contents at three temperature/pressure conditions. The error bars of the calculated unit cell volumes are given in parentheses. The wt % of H_2 for each configuration is given in Table III.

Temperature/pressure H_2 content	150 K/2 kbars		150 K/100 bars		273 K/100 bars	
	V	ρ	V	ρ	V	ρ
$0(s+m)+0\ell^a$	1218.1(3.0)	0.9544	1239.6(2.7)	0.9379	1275.3(3.8)	0.9116
$1(s+m)+0\ell^a$	1219.1(3.1)	0.9673	1239.6(3.2)	0.9513	1282.7(6.4)	0.9194
$1(s+m)+3\ell^b$	···		1244.6(3.1)	0.9110	1287.3(4.1)	0.8807
$1(s+m)+4\ell^b$	···		1244.0(2.7)	0.9123	1289.7(4.2)	0.8800
$1(s+m)+5\ell^b$	···		1244.4(3.0)	0.9130	1291.0(5.0)	0.8799
$1(s+m)+6\ell^b$	···		1249.7(2.4)	0.9099	1296.5(5.1)	0.8770
$1(s+m)+3\ell^c$	···		1245.6(2.7)	0.8738	1288.4(4.4)	0.8448
$1(s+m)+4\ell^c$	···		1246.2(3.1)	0.8751	1291.4(4.4)	0.8445
$1(s+m)+5\ell^c$	···		1249.1(2.9)	0.8749	1295.6(4.5)	0.8434
$1(s+m)+6\ell^c$	···		1256.3(3.0)	0.8716	1303.6(3.4)	0.8400
$1(s+m)+3\ell^d$	···		1247.4(2.7)	0.8482	1289.5(3.3)	0.8206
$1(s+m)+4\ell^d$	···		1247.7(3.5)	0.8504	1290.8(3.9)	0.8220
$1(s+m)+5\ell^d$	···		1250.4(2.8)	0.8510	1298.2(5.1)	0.8196
$1(s+m)+6\ell^d$	···		1258.4(4.0)	0.8478	1310.2(4.6)	0.8144
$2(s+m)+0\ell^a$	1263.5(3.6)	0.9464	1292.5(3.3)	0.9252	1382.4(7.7)	0.8650
$2(s+m)+3\ell^b$	1261.3(3.0)	0.9121	1287.1(3.7)	0.8938	1362.9(5.6)	0.8441
$2(s+m)+4\ell^b$	1264.4(2.8)	0.9107	1290.0(4.1)	0.8926	1369.9(7.4)	0.8406
$2(s+m)+5\ell^b$	1264.2(3.5)	0.9118	1291.2(2.7)	0.8927	1380.4(8.3)	0.8350
$2(s+m)+6\ell^b$	1271.4(2.7)	0.9075	1298.3(3.5)	0.8887	1412.2(16.1)	0.8170
$2(s+m)+3\ell^c$	1260.2(3.1)	0.8769	1286.7(2.8)	0.8588	1354.9(5.8)	0.8156
$2(s+m)+4\ell^c$	1260.6(2.5)	0.8784	1287.5(3.0)	0.8600	1357.0(5.5)	0.8160
$2(s+m)+5\ell^c$	1265.8(3.4)	0.8764	1293.4(3.3)	0.8578	1378.6(5.8)	0.8048
$2(s+m)+6\ell^c$	1279.9(3.2)	0.8686	1305.5(3.5)	0.8515	1404.4(14.8)	0.7915
$2(s+m)+3\ell^d$	1258.0(3.1)	0.8543	1285.3(3.1)	0.8362	1349.7(6.0)	0.7963
$2(s+m)+4\ell^d$	1261.8(3.1)	0.8541	1287.6(3.4)	0.8370	1352.0(6.9)	0.7971
$2(s+m)+5\ell^d$	1266.6(2.7)	0.8532	1293.7(3.6)	0.8353	1377.0(5.6)	0.7847
$2(s+m)+6\ell^d$	1282.8(3.4)	0.8447	1308.7(2.8)	0.8280	1412.3(16.7)	0.7672

[a]Large cages all occupied by MTBE.
[b]1/3 of large cages occupied by H_2 guests, 2/3 by MTBE.
[c]2/3 of large cages occupied by H_2 guests, 1/3 by MTBE.
[d]8/9 of large cages occupied by H_2 guests, 1/9 by MTBE.

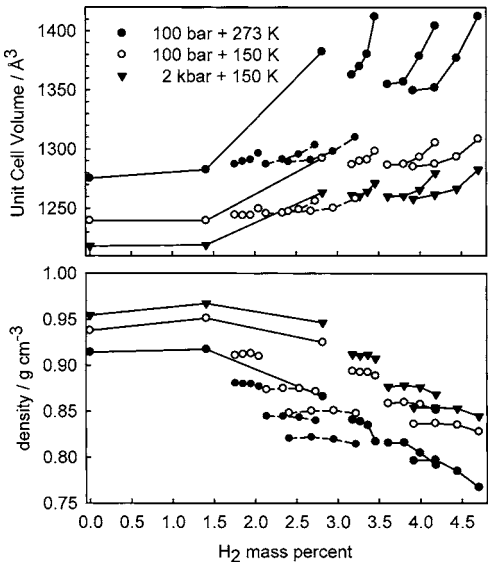

FIG. 9. The unit cell volume ($Å^3$) and density (g/cm^3) for binary MTBE $+H_2$ clathrates at 150 and 273 K temperatures and 100 bar and 2 kbar pressures for different occupancies of the cages with H_2 guests. The distribution of hydrogen guest molecules among the cages that corresponds to each hydrogen mass percent is given in Table III. Points with single occupancy of the $(s+m)$ cages are connected with dashed lines and points with double occupancy of the $(s+m)$ cages of the large cages are connected with solid lines.

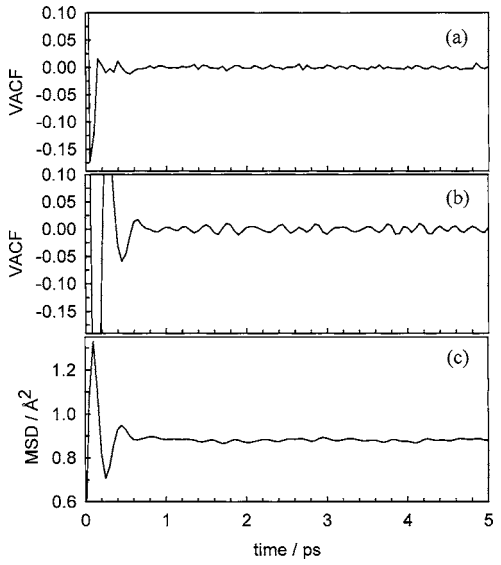

FIG. 10. (a) The velocity-autocorrelation function of the center of mass of the hydrogen guest molecules in doubly occupied $(s+m)$ cages. The collision time for the guests is less than 0.1 ps, and due to the collisions with the cage walls and the second guest molecule, the velocities of the hydrogen molecules becomes quickly randomized. (b) The velocity-autocorrelation function of the center of mass of the hydrogen guest molecules in singly occupied $(s+m)$ cages. The collision time for the hydrogen guests with the cage wall is ≈0.3 ps. The velocities of the hydrogen molecules change in a quasiperiodic manner as the guests undergo successive collisions with the cage. (c) The mean-square displacement of the center of mass of the hydrogen guest molecules in singly occupied $(s+m)$ cages. A period of ≈0.3 ps can be observed for the motion of the guests in the cages. Calculations in this figure are for configurations with MTBE in all large cages and at 150 K and 2 kbar pressure.

a decrease in energy of the unit cell when a single H_2 guest is placed in the s and m cages compared to the case where these cages are empty. This is understood with reference to Fig. 6 which shows that for a single H_2 guest the H_2–OW interactions are predominantly attractive. The energy of the unit cell increases sharply when a second H_2 guest is placed in the $(s+m)$ cages which can be related to the presence of the H_2–H_2 and H_2–OW repulsive interactions shown in Figs. 4 and 6.

The configurational energy of the unit cell increases when MTBE molecules in the large cages are substituted with sets of H_2 guests. This increase is observed in both single and double $(s+m)$ cage occupancies. This shows the stabilizing effect of the MTBE molecule on the clathrate structure and the repulsive contributions of the H_2–H_2 and H_2–OW interactions in the large cages. In the case of single occupancy of the $(s+m)$ cages, the configurational energy is not sensitive to the H_2 content of the large cages. For doubly occupied small cages and 150 K, the configurational energy is largely independent of the number of H_2 guests put in the large cages (up to the occupancy of five H_2 guests per large cage). At 273 K, the increased kinetic energy of the guests leads to a broadening of the RDF peaks and a sharper dependence of the configurational energy of the clathrates with the number of H_2 molecules placed in the large cages.

The unit cell volume and density for various MTBE and H_2 occupancies at 150 and 273 K temperatures and 100 bar and 2 kbar pressures are given in Table IV and plotted in Fig. 9. Results are shown for cases for single and double occupancies of the $(s+m)$ cages where all the large cages are occupied by MTBE and for cases where 1/3, 2/3, or 8/9 of the large cages are occupied by sets of three to six H_2 guests. In all three temperature and pressure conditions, there is a jump in the unit cell volume in going from single to double occupancy of the s and m cages. In the doubly occupied s and m cases, a further substitution of the MTBEs in the large cages with sets of H_2 molecules causes modest jumps in the unit cell volume. The volume jump becomes more pronounced for the high temperature simulations. A useful practical aspect of replacing the heavier MTBE molecules with lighter sets of H_2 guests in the large cages is that along with the substitution and increase in the mass percent of H_2 in the clathrate, the density of the material actually decreases.

The velocity-autocorrelation functions (VACFs) of the guest hydrogen molecules in the small and medium cages for double and single occupancies are shown in Figs. 10(a) and 10(b), respectively. These calculations are at 150 K and 2 kbar pressure for configurations where all the large cages are occupied by MTBE. The normalized VACF $C_v(t)$ is calculated in dimensionless form:

$$C_v(t) = \frac{\langle \mathbf{v}(0) \cdot \mathbf{v}(t) \rangle}{\langle \mathbf{v}(0) \cdot \mathbf{v}(0) \rangle}, \tag{3}$$

where $\mathbf{v}(t)$ is the velocity of the center of mass of the molecule. The Fourier transforms of VACFs of the guest hydrogen molecules for the single and double occupancies of the $(s+m)$ cages are shown in Figs. 11 and 12, respectively. The Fourier transform is presented both as a function of frequency (a) and the period (b) of the motion. The rattling motion of the guests in the cages for the singly occupied case, shown in Fig. 11, has two strong maxima at 3 and

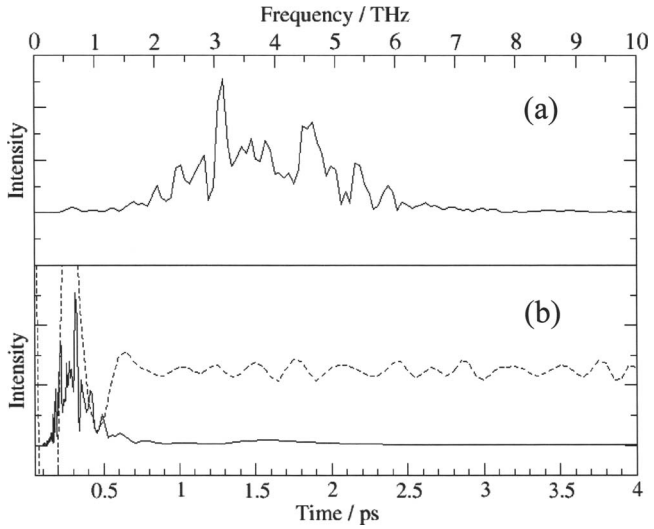

FIG. 11. (a) The Fourier transform of the velocity-autocorrelation function of the center of mass of the hydrogen guest molecules in singly occupied $(s+m)$ cages in the frequency domain. The two peaks at ≈3 and 4.5 THz (100 and 150 cm^{-1}, respectively) correspond to frequencies of the rattling vibrations of the hydrogen guests. (b) The Fourier transform of the VACF with the time abscissa along with the original VACF given for reference (dashed line). The rattling frequencies correspond to motions with periods of 0.2 and 0.35 ps.

4.5 THz, corresponding to periods of 0.35 and 0.2 ps, respectively. In the doubly occupied $(s+m)$ cages, Fig. 12, the combination of the motion in the cage and collisions between guest molecules leads to complex motion for which no distinct frequency arises. The collisions between the guests and the wall molecules randomize the velocity of the guests after a very short time period (<0.1 ps). Figure 12 suggests that the absorption corresponding to the motion of the hydrogen guests in the doubly occupied case will be broad and have no distinct features.

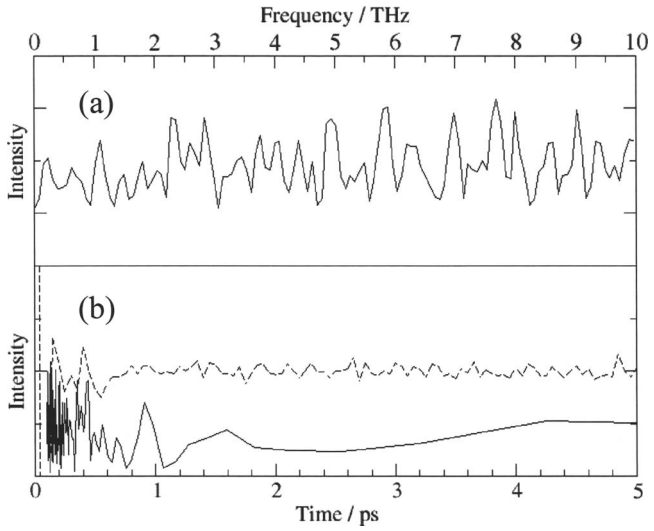

FIG. 12. (a) The Fourier transform of the VACF of the center of mass of the hydrogen guest molecules in doubly occupied $(s+m)$ cages in the frequency domain. The rattling motions along with collisions with guests in the same cage give a broad frequency spectrum which has no dominant adsorption maxima. (b) The Fourier transform of the VACF with the time abscissa along with the original VACF given for reference (dashed line).

The mean-square displacement (MSD) for the singly occupied small plus medium cages is shown in Fig. 10(c). The MSD for the guests is defined as

$$\Delta|\mathbf{r}(t)|^2 = \frac{1}{2}\left\langle \sum_{i=1}^{N} |\mathbf{r}_i(t) - \mathbf{r}_i(0)|^2 \right\rangle, \tag{4}$$

where $\mathbf{r}_i(t)$ is the location of the center of mass of molecule i at time t and the brackets $\langle\ \rangle$ represent an ensemble average. The quasiperiodic motion for the guests seen in the VACF for the singly occupied cages is observed in the MSD curves as well.

IV. SUMMARY AND CONCLUSIONS

Binary H_2+MTBE structure H clathrates with single and double occupancies of H_2 in the small and medium cages and different fractions of H_2:MTBE in the large cages are studied with molecular dynamics simulations in a range of temperatures and pressures corresponding to experimental conditions.

There is a large increase in the unit cell volume and inclusion energy as the small cages accept second hydrogen guest molecules. The RDF for H_2-H_2 guests in doubly occupied small and medium cages (Fig. 3) shows that interaction among the two guest molecules is primarily repulsive. In contrast the interactions between up to six H_2 guests in the large cages remain mostly attractive (Fig. 4).

Substitution of MTBE molecules with sets of H_2 guests increases the energy of the system (see Fig. 8). At low temperatures this increase is relatively insensitive to the number of guest hydrogen molecules placed in the large cages (up to six hydrogen molecules). At higher temperatures, the energy and unit cell volume become strongly dependent on the number of hydrogen guests placed in the large cells. A similar behavior is seen in the binary H_2+tetrahydrofuran (THF) structure II clathrate[11(b)] where the substitution of the THF molecule in the large cages with sets of four H_2 guests increases the unit cell energy.

In both the MTBE and THF binary hydrogen clathrates, the organic guest molecules stabilize the clathrate structure and allow the synthesis of the hydrogen-containing clathrate to occur at much lower pressures than is needed to synthesize the pure hydrogen clathrate. The disadvantage of incorporating these secondary guests is that they make up a relatively large weight percentage of the final binary hydrogen clathrate product.

In this work, quantum effects have been neglected in considering the H_2-H_2 and H_2-H_2O intermolecular interactions since the lowest temperature considered is 150 K. In the second virial coefficient, there is an overall positive contribution from the sum of corrections for quantum statistics and terms up to the order of $\hbar^4$.[27,28] This quantum effect causes an extra repulsion in the H_2-H_2 interaction which is reflected in the fact that the second virial coefficient is more positive in quantum gases than in their classical analogs. This extra repulsion will affect the hydrogen configurational energy at low temperatures.

The rotational wave functions of *ortho-* and *para-*hydrogen have different symmetries and interact differently

with adsorbed surfaces.[29–32] *Para*-hydrogen has a spherically symmetric wave function and interacts through a spherically symmetric isotropic potential with the other surface atoms and molecules. The wave function of *ortho*-hydrogen, on the other hand, is shaped like a hydrogen *p* orbital and has anisotropic interactions with other molecules on the surface. A similar phenomenon may be expected to occur for hydrogen adsorbed in clathrate cages. At low temperatures, these symmetry effects can cause preferential adsorption in certain cage sites or preferential choice of certain occupancy numbers in the cages. Path integral Monte Carlo (PIMC) simulations[33] can be performed to include these symmetry related quantum effects, along with other quantum effects such as zero-point energy and electron dispersion.

ACKNOWLEDGMENT

This work was supported by the National Research Council of Canada Fuel Cell Initiative.

[1] K. A. Udachin, C. I. Ratcliffe, G. D. Enright, and J. A. Ripmeester, Supramol. Chem. **8**, 2732 (1997).
[2] D. W. Davidson, S. R. Gough, Y. P. Handa, C. I. Ratcliffe, J. A. Ripmeester, and J. S. Tse, J. Phys. (Paris) **48**, C1-537 (1987); J. A. Ripmeester, J. S. Tse, C. I. Ratcliffe, and B. M. Powell, Nature (London) **325**, 135 (1987).
[3] R. M. Pratt, D.-H. Mei, T.-M. Guo, and E. D. Sloan, Jr., J. Chem. Phys. **106**, 4187 (1997).
[4] W. L. Mao, H.-K. Mao, A. F. Goncharov, V. V. Struzhkin, Q. Guo, J. Hu, J. Shu, R. J. Hemley, M. Somayazulu, and Y. Zhao, Science **297**, 2247 (2002).
[5] Yu. A. Dyadin, E. G. Larianov, A. Yu. Manakov, F. V. Zhurkov, E. Ya. Aladko, T. V. Mikina, and V. Yu. Komarov, Mendeleev Commun. **9**, 209 (1999).
[6] W. L. Mao and H.-K. Mao, Proc. Natl. Acad. Sci. U.S.A. **101**, 708 (2003).
[7] K. A. Lokshin, Y. Zhao, D. He, W. L. Mao, H.-K. Mao, R. J. Hemley, M. V. Lobanov, and M. Greenblatt, Phys. Rev. Lett. **93**, 125503 (2004).
[8] L. J. Florusse, C. J. Peters, J. Schoonman, K. C. Hester, C. A. Koh, S. F. Dec, K. N. Marsh, and E. D. Sloan, Science **306**, 469 (2004).
[9] H. Lee, J.-W. Lee, D. Y. Kim, J. Park, Y.-T. Seo, H. Zeng, I. L. Moudrakovski, C. I. Ratcliffe, and J. A. Ripmeester, Nature (London) **434**, 743 (2005).
[10] J. A. Ripmeester and H. Zeng (private communication).
[11] (a) S. Alavi, J. A. Ripmeester, and D. D. Klug, J. Chem. Phys. **123**, 024507 (2005); (b) S. Alavi, J. A. Ripmeester, and D. D. Klug, *ibid.* **124**, 014704 (2006).
[12] H. J. C. Berendsen, J. R. Grigera, and T. P. Straatsma, J. Phys. Chem. **91**, 6269 (1987).
[13] *CRC Handbook of Chemistry and Physics*, 83rd ed., edited by D. R. Lide (CRC, Boca Raton, FL, 2002).
[14] E. P. van Klaveren, J. P. J. Michels, J. A. Schouten, D. D. Klug, and J. S. Tse, J. Chem. Phys. **114**, 5745 (2001); **115**, 10500 (2001); **117**, 6636 (2002).
[15] A. D. Becke, J. Chem. Phys. **98**, 5648 (1993).
[16] M. J. Frisch, G. W. Trucks, H. B. Schlegel *et al.*, GAUSSIAN 98, Revision A.7, Gaussian, Inc., Pittsburgh, PA, 2001.
[17] C. M. Breneman and K. G. Wiberg, J. Comput. Chem. **11**, 361 (1990).
[18] W. D. Cornell, P. Cieplak, C. L. Bayly, I. R. Gould, K. M. MerzJr., D. M. Ferguson, D. C. Spellmeyer, T. Fox, J. W. Caldwell, and P. A. Kollman, J. Am. Chem. Soc. **117**, 5179 (1995); see also http://amber.scripps.edu
[19] S. Nosé, J. Chem. Phys. **81**, 511 (1984).
[20] W. G. Hoover, Phys. Rev. A **31**, 1695 (1985).
[21] S. Melchionna, G. Ciccotti, and B. L. Holian, Mol. Phys. **78**, 533 (1993).
[22] DLPOLY 2.14, edited by T. R. Forester and W. Smith, CCLRC, Daresbury Laboratory, 1995.
[23] D. Frenkel and B. Smit, *Understanding Molecular Simulation* (Academic, San Diego, 2000).
[24] M. P. Allen and D. J. Tildesley, *Computer Simulation of Liquids* (Oxford Science, Oxford, 1987).
[25] D. C. Rapaport, *The Art of Molecular Dynamics Simulation* (Cambridge University Press, Cambridge, 1995).
[26] J. D. Bernal and R. H. Fowler, J. Chem. Phys. **1**, 515 (1933).
[27] J. O. Hirschfelder, C. F. Curtiss, and R. B. Bird, *Molecular Theory of Gases and Liquids* (Wiley, New York, 1967).
[28] D. A. McQuarrie, *Statistical Mechanics* (Harper & Row, New York, 1976).
[29] D. White and E. N. Lassettre, J. Chem. Phys. **32**, 72 (1960).
[30] I. P. Silvera and M. Nielsen, Phys. Rev. Lett. **37**, 1275 (1976).
[31] V. Buch and J. P. Devlin, J. Chem. Phys. **98**, 4195 (1993).
[32] Q. Wang and J. K. Johnson, J. Chem. Phys. **110**, 577 (1999).
[33] D. Chandler and P. G. Wolynes, J. Chem. Phys. **74**, 4078 (1981); B. Berne and D. Thrimulai, Annu. Rev. Phys. Chem. **37**, 401 (1986); J. D. Doll, D. L. Freeman, and T. L. Beck, Adv. Chem. Phys. **78**, 61 (1990).